Carleton University
Dept. of Mechanical and Aerospace Engineering

MAAE 4907 C
Prof. M. El Sayed
Prof. P. Liu
Prof R. Liu

Written By:
Eithin Pero
101203184

Reviewed By:

Report #: BWB25-TR2-5.7.2

SYSTEMS ENGINEER - 2

WINTER 2025 TECHNICAL REPORT

ABSTRACT

This document describes the work accomplished in the winter semester by the Systems Engineer on the Peregrine 1, a blended-wing body unmanned aerial vehicle (BWB UAV). The current design challenges for the Peregrine 1 include the use of additive manufacturing to construct the platform, solar powered flight, and a mapping mission. The finished mapping module is presented in Section 2.0, the design, analysis, challenged faced, and produced products for the landing gear system is outlined in Section 3.0. The design, testing, and validation of the elevon assembly method and actuation linkage are described in Section 4.0.

TABLE OF CONTENTS

LIST OF TABLES

LIST OF FIGURES

NOMENCLATURE

BWB	Blended Wing Body
CFD	Computational Fluid Dynamics
CG	Center of Gravity
FEA	Finite Element Analysis
FOV	Field of View
G	Acceleration Relative to Standard Acceleration due to Earth's Gravity
GCP	Ground Control Point
GPS	Global Positioning System
GSD	Ground Sample Distance
ID	Inner Diameter
IMU	Inertial Measurement Unit
KTAS	Knots True Airspeed
LiDAR	Light Detection and Ranging
LG	Landing Gear
MB	Megabyte
MLG	Main Landing Gear
MP	Megapixel
MSDO	Multiscale Design Optimization
NIR	Near Infrared
NLG	Nose Landing Gear
OD	Outer Diameter
OML	Outer Mold Line
P1	Peregrine 1
PETG	Polyethylene Terephthalate Glycol
RGB	Red, Green, Blue
SHCS	Socket Head Cap Screw
UAV	Unmanned Aerial Vehicle
VTOL	Vertical Takeoff and Landing

1.0 INTRODUCTION

The project objective of the 2024-25 BWB UAV capstone is to design, test, build and fly a solar powered, unmanned aerial vehicle. The blended-wing body configuration of the Peregrine 1 has many benefits for an unmanned, long endurance mission. A blended-wing body aircraft has a seamless transition between the wing and fuselage, similarly to a flying wing configuration. Contrary to a flying wing, a blended-wing body design retains some semblances to a traditional aircraft by keeping most of the interior volume within the fuselage potion of the body. This design improves the aerodynamic characteristics of the aircraft, allowing the fuselage to generate more life than the fuselage of a conventional aircraft, improving fuel efficiently [1].

The major design challenges placed upon this year's design are the requirements of additive manufacturing, increased flight duration via solar panels, and an optimization of the structure using MSDO principles. The blended wing body UAV employs a conventional takeoff and landing with a single pusher configuration. The Systems Engineer 2 on the team is tasked with the following objectives:

1. Analyzes and designs the landing gears to airframe integrations and potentially the deployment and retraction system of the landing gears.
2. Analyzes and designs the control surfaces and their integration into the airframe.
3. Analyzes and designs the mapping module and its integration into the platform.
4. Analyzes and designs the steering system and its integration into the platform

Through the course of the semester, each task was completed to a usable state. The MLG, mapping system, and control surface integration was very successful. For the NLG, a few flaws persist.

2.0 MAPPING MODULE

For the MAPIR Survey3 mapping camera selected in the Fall semester, the integration and mounting method was designed. Additionally, considerations were made for the integration to the flight controller.

2.2 Camera Specifications

The camera selected by the Systems 1 Engineer is the MAPIR Survey3W, RGN [2]. Research was conducted on critical sensor parameters in the fall semester which was handed off to the Systems 1 Engineer for the selection. More information on the specifications and validation, refer to the Systems 1 Engineer Winter technical report.

2.1 Camera to Airframe Integration

For camera integration, a physical mount was designed to support the camera and isolate it from the aircraft vibrations. The mount was based on the Pixhawk isolation platform, which uses two parallel platforms connected at all four corners with a rubber grommet [3]. The platform, shown in Figure 1 and Figure 2: Side view of the Survey3W camera mounted to the isolation platform below, was modelled from scratch to be manufactured with additive manufacturing.

Figure 1: Top view of Camera Mount with MAPIR Survey3W

Figure 2: Side view of the Survey3W camera mounted to the isolation platform

Since the photos in Figure 1 and Figure 2 were taken, a problem was identified where the raised *power* button on the camera interacted with the surface of the top plate, causing the camera to rapidly turn off and on. This has since been rectified with a circular cutout where the button interacts with the mount. Due to the inaccuracies associated with 3D printing, drilling the mounting holes to size in post-processing is preferred. Four M4x8mm screws with flat washers are used to secure the assembly to a raised extrusion in the belly of the Peregrine 1, shown in Figure 3 below, which is fitted with M4 heat set inserts.

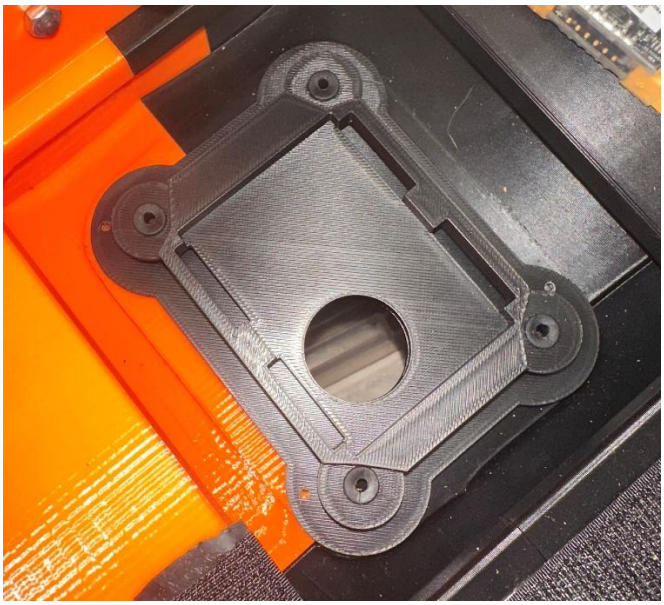

Figure 3: Floor cutout and raised extrusion for the mapping module

2.1.1 Vibration Testing

To validate the isolation system, a vibration test incorporating a sine sweep through vibration frequency ranges most applicable to the aircraft was considered, but due to time constraints and availability, it was never completed.

A vibration test with a sine sweep vibrates the assembly through a range of frequencies to see if the assembly or component vibrates at any specific frequencies. This method is often used in industry to validate flutter simulations and operational frequencies on aircrafts [4]. It is theorized that the degree of pretension in the rubber grommets will directly correspond to an alteration in the resonant frequencies on the assembly. Additionally, this testing will verify that the purchased rubber grommets work at all.

For more information regarding vibration testing, refer to the Dynamics Engineers winter report.

2.3 Camera to Avionics Integration

The camera integration to avionics includes the GPS, power, and sensor trigger. It was decided to use the integrated GPS and power for the MAPIR camera to reduce the complexity.

The battery that comes with the MAPIR camera is a removeable 1200mAh Li-ion, that supports 150 minutes of continuous footage. For a short flight test, the removable battery is sufficient. For longer missions, the camera can be connected to the Pixhawk via a USB cable and draw power directly from the onboard battery.

Regarding the GPS data required for geotagging each image, integration into the flight controller is possible, but likely involved. For the purposes of the flight test mission, the GPS attachment that came with the MAPIR battery is sufficient.

3.0 LANDING GEAR

In the fall semester, a weighted trade study was performed between a fixed landing gear, and two configurations of a retractable landing gear. It was determined that the additional time needed for the research, design, and testing needed to deliver a retractable landing gear was a significant risk for the success of the project. The author worked extensively on the Catia model in the fall, delaying systems related work.

It was evaluated with advice from the Aerodynamics Engineer, that at the mission profile cruise speed of 65 KTAS, the effects of the landing gear system on drag would be minor. A study on the trade-off between the reduced mass of the fixed landing gear with its increased drag, and the increased mass of the retractable landing gear with its reduced drag, on the thrust required was intended to be performed. Due to delays with the model required with CFD, this was put on hold.

To reduce risk on the success of the mission, a fixed landing gear configuration was pursued.

3.1 Global Geometry and Positioning

In the design of the landing gear, one of the fixed design constraints was the lateral positioning of the ground contact points. This parameter heavily affects the overturn angle of the aircraft, and thus, the stability of the aircraft in taxi, takeoff, and landing. Additionally, the wing incidence is an important parameter that describes the angle of attack of the wings, as the aircraft is on the ground, which affects the lift that can be generated and the rotation on takeoff [5]. It was identified early in the design that these parameters should be held constant from the previous design analysis to preserve these aerodynamic and performance characteristics.

3.1.1 Sizing Procedure

For the tricycle landing gear configuration on the Peregrine 1, the book *Aircraft Design* by Daniel Raymer was consulted to adequately position the gears [6]. By starting with the global geometry of the gears, the design space and constraints required for the landing gear would be properly defined to begin finalizing the local geometry of the gears. With non-applicable steps omitted, the general positioning follows the following process:

1. Draw the forward and aft CG-limit on a side view of the aircraft, along with the mean geometric cord.
2. Draw a prop-strike limit line, horizontal to the ground.
3. Draw a tail strike line measured 15 degrees from the ground.

   Note: The prop strike limit as per 14 CFR 23.925(a) is 7 inches [7]. This is a requirement that ensures that prop clearance is maintained while accounting for flat tires and strut compression. For this selection the prop-strike limit was chosen based on if the foam portion of the wheels were deflected completely. The prop-strike limit found is 0.68 inches, where the distance between the axle hole and the bottom of the strut is 0.291”, the diameter of the wheel hub is 1” and the radius of the selected tire is 1.18”. The maximum strut compression of 1.5 inches was added to this distance for a total prop-strike clearance of 2.18 inches.

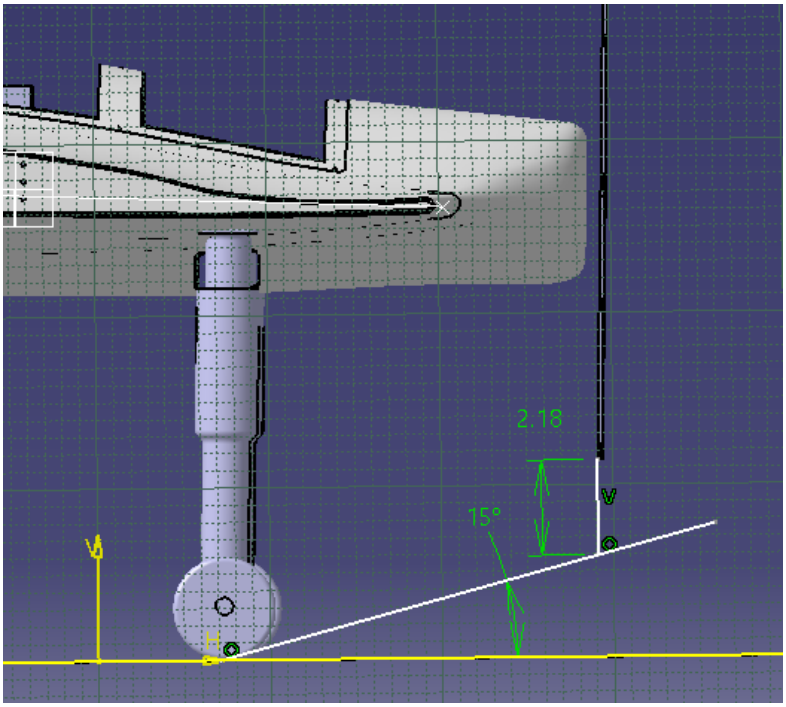

Figure 4: Prop-strike and tail strike limit on the Peregrine 1 model

4. Draw a line through the CG, perpendicular to the trail-strike line.
5. Where the tail strike line meets this line, draw a vertical line through this intersection. This point is the ground contact point of the MLG.
6. Position the NLG such that the load carried by it is no more than 20% of the aircraft weight when the CG is at the forward position, and no less than 10% when the aircraft is at the aft limit.

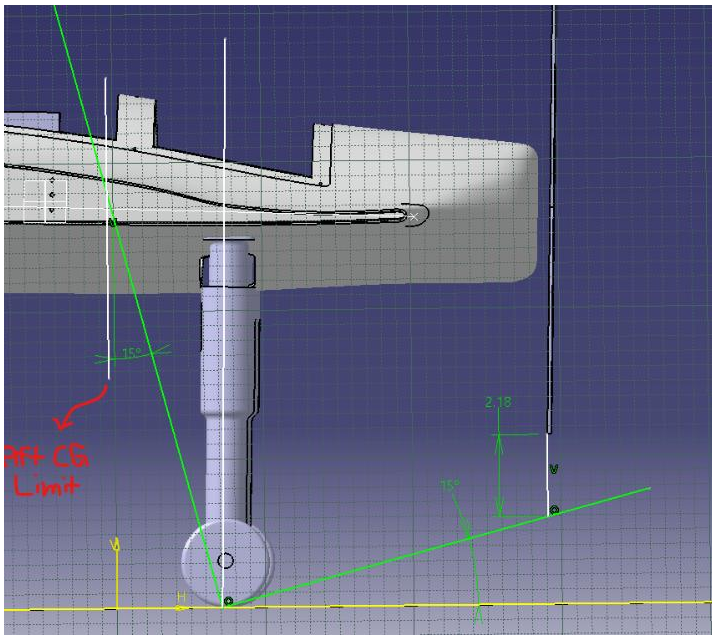

Figure 5: Aft CG limit of Peregrine 1

This sizing was conducted before the position of the CG was known. The following parameters and methodology were used in conjunction to the sizing steps listed above:

1. Since the CG limits were not known at the time of sizing, the approach suggested by Raymer could be applied backwards, guiding the future positioning of the aft and forward CG limits, instead of using the known CG limits to position the landing gears.
2. The CG can be manipulated with the positioning of internal components. The previous years longitudinal position of the main landing gear will be maintained.
3. If the lateral positioning of the ground contact points of the new landing gear are maintained from the previous years (5.5 inches from centerline), the overturn angle does not need to be reconsidered.
4. Once the aft and forward CG is determined from the Masterlines Engineer, the NLG can be repositioned to satisfy step 6 of landing gear positioning.
5. The sizing was conducted considering a 12-inch propellor.

3.1.2 Relative Sizing of NLG

Once the height of the MLG was determined using Raymers approach, the relative sizing of the NLG was still missing. In a normal sizing procedure, the aircraft's longitudinal axis and ground attitude is already known from the performance analysis. The longitudinal axis runs from the tip to the tail of the plane, through the CG. The aircraft's ground attitude measures the angle between the longitudinal axis and the ground, while it is resting on the ground.

An aircrafts ground attitude is crucial for a plane due to the downstream effects of its positioning. For example, the wing angle of incidence describes the fixed angle between the wings chord line at the root and the aircrafts longitudinal axis. In the conceptual design phase, if this angle is determined to be 2° for the aircraft to have the required performance through its mission profile, its position relative to the ground must also be known. If the nose gear is constructed too short, and aircraft sits pitched down on the runway, the realized angle of attack would then be negative and would impact stall angle on landing and lift generated on takeoff.

For the Peregrine 1, conceptual design parameters like these could not be found. The assumption was made that the conventional foam model that was used in the last flight test of the project, shown in Figure 6 below, would have the required ground attitude when the landing gear that was designed for the platform was installed.

Figure 6: Foam Peregrine 1

From measurements made on the aircraft, the following parameters were found, tabulated in Table 1 below.

Table 1: Measured and calculated parameters for the foam Peregrine 1

Parameter	Value
Distance from tail to MLG	9”
Distance from tail to NLG	23”
Distance between MLG ground contact points	13.25”
Distance from tail to ground	9”
Distance from MLG-fuselage mounting plate to ground	7”
Distance from NLG-fuselage mounting plate to ground	7”
Distance from ground to wing chord line (at the root) on the trailing edge	8.75”
Distance from ground to wing chord line (at the root) on the leading edge	9.5”
Wing angle of incidence (with the longitudinal axis running from the center of the nose to the center of the tail)	1.66°
Angle of attack (on takeoff)	2.06° (+ elevon deflection)

With the angle of incidence and angle of attack on takeoff determined from the physical foam model, the current Peregrine 1 model was positioned relative to the ground accordingly, and the NLG and MLG were designed and modelled in reference to this constraint. Figure 7 shows a measurement being taken on the foam model and Figure 8 displays the model being constrained relative to the ground via the angle of attack determined from measurements taken on the foam model.

Figure 7: Ground to wing chord line on leading edge measurement for the foam Peregrine 1

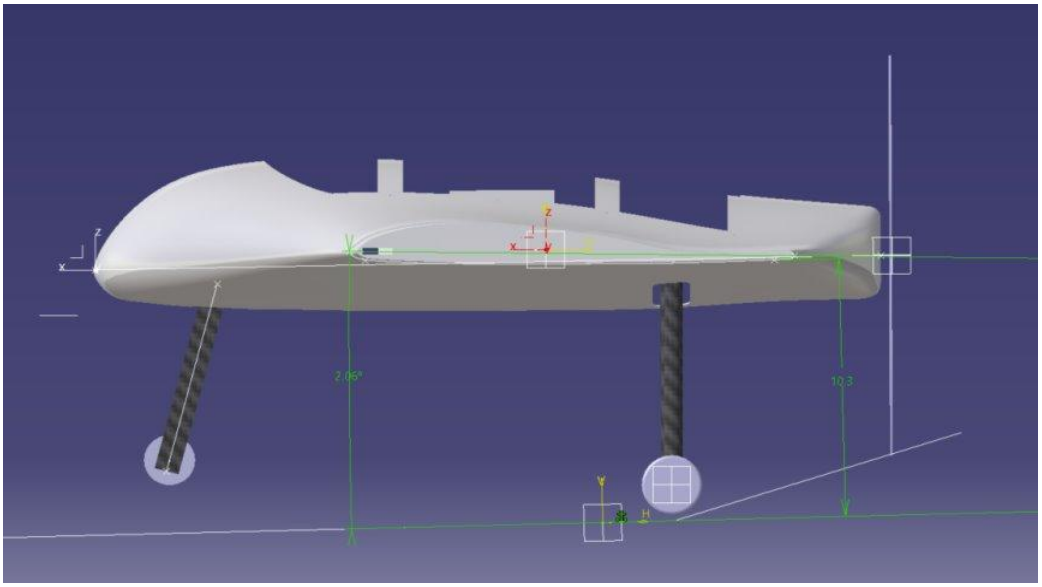

Figure 8: Positioning of the CAD model for subsequent design of LG

3.1.3 Accomplishments and Notes

For the 2024-2025 capstone year, steps 1 through 5 of the sizing were completed, and the produced landing gear follows these dimensions. Step 6 of positioning the NLG was not completed as the CG was not determined until very close to the end of the semester. Additionally, it was found after the sizing was completed that a 14-inch propellor was required to produce the required thrust. A 14-inch propellor was used on the platform in subsequent testing. Additionally, the vertical positioning of the LG-fuselage mounting platforms changed slightly, and the required height of the LG was not reevaluated. Recommendations will be discussed in Section 3.5.

3.2 MLG Design

From the beginning of the project, it was known that a custom main landing gear would be required. There were initial concerns about the weight of the platform resulting from the additive manufacturing of the airframe and skin. Initial estimates put the platform at 25kg or higher for print material only.

Off-the-shelf landing gear struts rated for this platform weight cost $650 and above [8]. The cost of these systems made a custom MLG very inciting.

This section presents a timeline of iterations for future reference in Section 3.2.1, an analysis of shock loads, spring selection, and damping considerations in Sections 3.2.2 and 3.2.3, and an overview of the produced design in Section 3.2.4.

3.2.1 Iterations

The MLG was through many iterations over the course of the design phase. A summary of these iterations is presented below as a reference for future years.

From the fall semester, 3 configurations were being considered, shown in Figure 9 below.

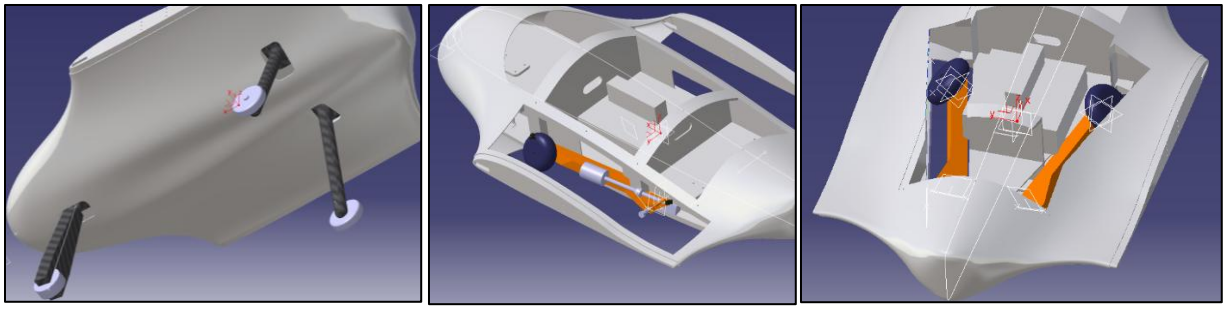

Figure 9: Fixed LG model (Left), retractable MLG configuration 2 (middle), retractable configuration 1 (right)

Initially, the retractable configuration 2 was going to be pursued for its advantages regarding aerodynamics, but due to the work on the Catia model with the master manufacturing engineer in the fall, it was decided that with the reduced time available there would be less risk to the success of the project with a fixed gear. Additionally, due to a slow start with the CAD model and the downstream effects of a slow start for the stress and structure engineers, the implications of cutting structural material out of the root fairing, which was the proposed housing space for the retractable gear, could not be realized.

For more information regarding the retractable gear mechanism, refer to the Systems 2 Fall Technical Report [9].

With a fixed configuration selected, spring and damping mechanisms needed to be designed alongside the geometry of the gear. A starting point for the spring mechanism was proposed by the Systems Engineer in 2021-2022, shown below in Figure 10.

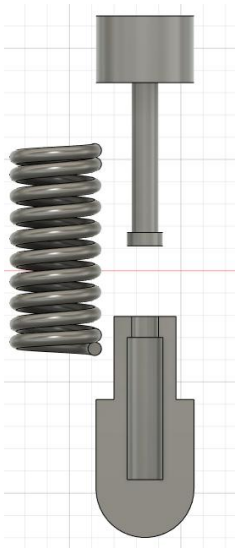

Figure 10: 2021-22 VTOL landing gear shock mechanism [10]

The design suggests a 0.813” OD compression spring goes on the exterior of a piston cylinder assembly. Two key characteristics that warranted a redesign of the mechanism were that the piston size is 6 mm and on full extension of the mechanism, only a very small length of material holds the plunger vertical. For the current project objective of additive manufacturing, a rod this small would shear easily if any instability is introduced in the mechanism.

From an analysis of the VTOL landing gear, it was determined that multiple contact points between the piston and outer cylinder would be necessary to keep the relative position of the two components concentric. Figure 11 below shows the modifications made to the landing gear spring housing. Since the inner diameter of a reasonably sized spring for the application is a small constraint to fit an inner piston and outer cylinder through, the outer cylinder was moved to the outside of the spring. The gap made between the two major components of the strut houses the compression spring, which transfers the load to well supported regions of the inner and outer cylinders.

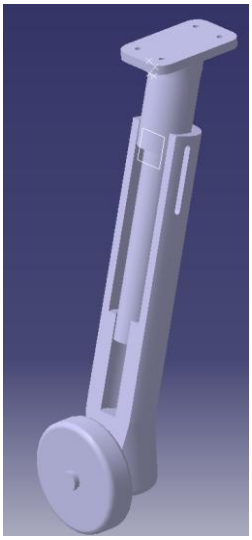

Figure 11: Piston cylinder mechanism for landing gear compression spring

Additionally, this design ensures that the two concentric bodies are always in contact with each other at two locations at a distance equal to or greater than the length of the spring. This design reinforces the ability for the two components to maintain their concentricity with each other, reducing frictional loading and the potential for one component to shear independently from the other.

The last major design change to be made in the design process was the change from a laterally angled gear to a perfectly vertical gear. It was found that additively manufactured PET-G is stronger in compression than in tension, with an ultimate tensile strength of 20-25 MPa and a compressive strength of 51-68 MPa [11]. Due to this, it was desirable for bending stress to be eliminated from the design. Through consultation with the master manufacturing engineer, it was determined that while maintaining the ground contact points of the gear, a vertical gear would be inline with the fuselage frames. With potential attachment structure available for the mounting points of the MLG, a vertical gear was pursued.

3.2.2 Spring Selection

For the characterization of the dynamics of the system, it was attempted to use the second-order linear ODE for a spring-mass-damper system, described in Equation 1 below.

$$m\ddot{x} + c\dot{x} + kx = F(t) \quad (1)$$

Little progress was made in this avenue due to the limited parameters known about the system. The determination of the damping coefficient is usually determined from recording the physical behaviour of the system. The forcing function described by F(t) is also a difficult parameter to obtain and estimate.

There are cases where this function is estimated as a damped sine wave, matching the diminishing oscillatory behaviour of the system upon landing.

The methodology used to size the springs was using landing loads simulated by the Loads Engineer. In the early stages of modelling, MSC Adams was giving max deceleration forces between 2G and 100G at a landing sink rate of 3m/s. Five sets of springs were purchased with a range of stiffness values to allow for testing. To determine the range needed, a G-force was used in conjunction with an estimated aircraft mass of 25kg to determine the peak force seen in the gear. The reason for the discrepancy between the final aircraft mass of 13kg and the assumed value of 25kg was due to the still present fears of an oversized aircraft. 25 kilograms represents the maximum weight drone that do not require Special Flight Operations Certificate in Canada, which would have meant an immediate scrub of all planned testing [12]. From the maximum force seen in the gear, Hooke's Law was used to determine the stiffness required for the spring to experience its maximum compression under the hard landing load. A summary of these calculations is provided in Table 2 below. A sample calculation for the first row is provided in Equation 2 and 3 below.

$$F = 9.81\left[\frac{m}{s}\right] * 2G * 12.5[kg] = 245.25[N] \quad (2)$$

$$k = \frac{F}{x} = \frac{245.25[N] * \left(\frac{0.22489\left[lb_f\right]}{1\,[N]}\right)}{1.5[in]} = 36.7\left[\frac{lb}{in}\right] \quad (3)$$

Table 2: Spring stiffness parameters, calculations, and values

Maximum G-loading from MSC Adams	Assumed Aircraft mass (mass per gear)	Maximum force experienced	Assumed maximum deflection	Spring stiffness required
2G	25kg (12.5kg)	245.25 [N]	1.5 [in]	36.76 [lb/in]
10G	25kg (12.5kg)	1226.25 [N]	1.5 [in]	183.9 [lb/in]
25G	25kg (12.5kg)	3065.62 [N]	1.5 [in]	459.6 [lb/in]
50G	25kg (12.5kg)	6131.25 [N]	1.5 [in]	919.2 [lb/in]

From the calculations in Table 2, springs were sourced from McMaster-Carr whose sizing fit the strut mechanism and whose spring rate were between the calculated range. The highest spring stiffness available for a spring that is within the dimensions of 2.5" long, 1" OD, and less than 0.75" ID was 220 lb/in, which is a sanity check that if there are impact loads on the aircraft exceeding 15G, it should be rectified by other means. This information was given back to the Loads Engineer. A placeholder for the inner and outer cylinders used for validation of the fit of the spring is shown below, in Figure 12.

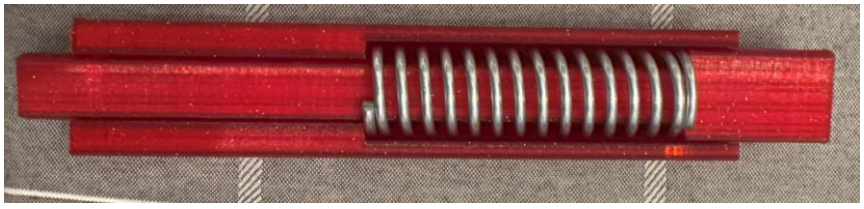

Figure 12: Placeholder strut for mechanism validation

The purchased springs are listed in Table 3 below.

Table 3: Purchased Spring Parameters

Spring rate [lb/in]	OD	ID	Uncompressed Length	Compressed Length	McMaster Carr Number
35 (experimentally determined)	1”	0.85”	3.5”	~1.5”	N/A (Ottawa Fasteners)
54.68	1”	0.76”	2.5”	1.63”	9657K32
78	1.031”	0.781”	3”	2.28”	9620K32
95	1.031”	0.781”	2.5”	1.91”	9620K31
220	1.031”	0.719”	2.5”	2.03”	9620K41

The spring with a spring constant of 78 lb/in was accidently ordered instead of the equivalent one with a length of 2.5”.

When the information of total aircraft weight was released by the Master Manufacturing Engineer as 13kg, the purchased springs were further analyzed for their applicability. Additionally, the Loads Engineer performed a drop test, discussed further in Section 3.5, that yielded an expected maximum G loading on the platform between 12G and 23G. The purchased springs of 2.5 inches in length were used in the calculation of the maximum G-loading they could take on landing before they bottom out.

Table 4: G-loading at max compression and percent stroke deflection under static loading for purchased springs

Spring rate [lb/in]	Stroke length	Force at maximum compression	Mass per MLG [kg]	G-loading at max compression	% Stroke deflection under static aircraft load
54.68	0.87”	211.6 [N]	6.5	3.32	30%
95	0.59”	249.3 [N]	6.5	3.91	26%
220	0.47”	459.4 [N]	6.5	7.20	14%

Considering the G-loading at max compression indicates that the 220lb/in spring would be ideal for the aircraft if only the hard landing loads provided by the Loads Engineer is considered. For smooth landings, where say 50 N is experienced, such a high spring rate will restrict the travel of the gear to a fraction of the total available stroke, reducing the efficiency of the friction damping, described in section 3.2.3. For this reason, the spring with a spring constant of 95lb/in was selected.

3.2.3 Damping Parameters

Damping is broadly defined as the restraining of vibratory motion, such as mechanical oscillations, etc., by dissipation of energy [13]. For the landing gear, damping is desired to decrease the energy acquired by the transfer of vertical decent speed to the gears. An ideal spring-mass system, with no energy losses, will indefinitely oscillate. For the landing gear, this means bouncing on landing which can cause a loss of control before the aircraft is brought to rest.

Damping can be introduced through a variety of mechanisms. In large aircraft, this is usually done via viscous damping in oleo struts, where viscous fluid is pushed through small orifices which restricts the velocity of the stroke. On the first cars, damping was introduced on the leaf struts through a friction disk

shock absorber [14]. In these shock absorbers, the mechanism of damping is provided by friction, where concentric disks are fastened together restricting the speed that the axles can move relative to the body of the car. Damping can also exist as an inherent property of a material. As a material is elastically deformed, some of the energy is dissipated through heat. Viscoelastic materials like rubber, foams, and some polymers are very efficient at dissipating energy through heat when deformed.

At the start of the semester, an article was found describing the use of polymer disks as a complete shock and damping solution for a light aircraft [15]. Further information regarding this design was unable to be found. It was proposed that a viscoelastic material could be purchased, tested as per ASTM D3574 to determine the hysteresis energy loss, and size it to the landing gear system. Foam was purchased, shown in below, but was not of the correct size for proper testing.

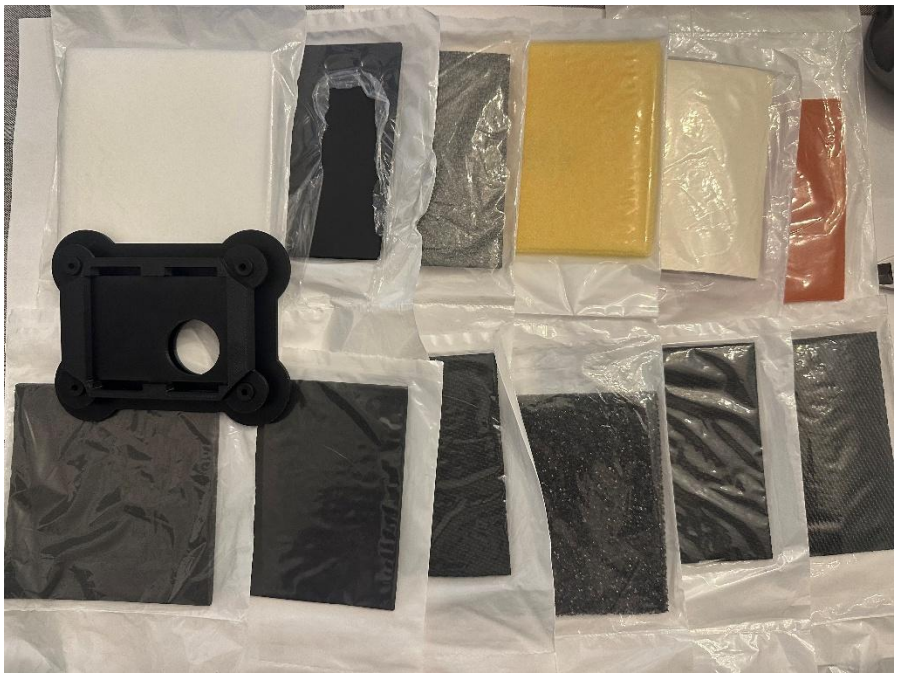

Figure 13: Foam purchased for energy testing (mapping mount for scale, Mcmaster-Carr 2172T22)

Instead, the implantation of friction damping was pursued. By measured the difference between the radii of the outer and inner cylinder, where they contact, the arc length of the slot was calculated to provide an adequate distance for the outer cylinder to sinch the inner cylinder using 1” hose clamps. The frictional force imparted by tightening the hose clamps was set empirically.

3.2.4 Final MLG

The final iteration of the MLG assembly is composed of the inner and outer cylinders, a partially threaded M3x65mm bolt that serves as the axle, and a shear bolt assembled through a slot existing on the outer cylinder that is fastened into the inner cylinder, preventing relative rotational movement between the two cylinders. A diagram of the 3D printed components is shown in Figure 14 below.

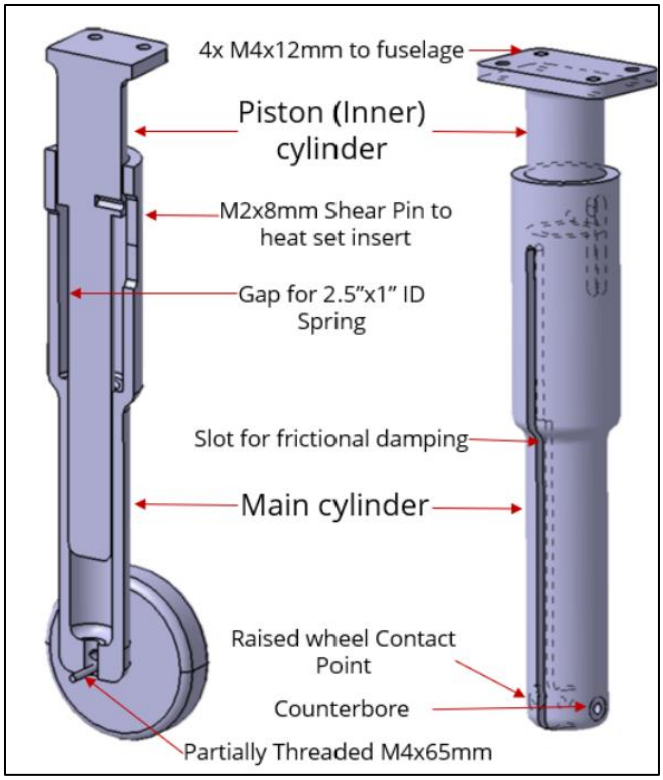

Figure 14: Diagram of MLG features on a full and section-view model

At the axle hole, the inside of the outer cylinder has a small counterbore allowing the M3 hex nuts securing the assembly to reduce their profile relative to the wind. On the wheel side of the outer cylinder, a small, curved protrusion is present, allowing the wheel to sit 3mm offset from the edge of the strut. By making this protrusion curved, the contact between the flat washer, which sits between the wheel and the strut, has minimal contact with the plastic, reducing friction.

The selection of a partially threaded M3 bolt as the axle was to allow the hub of the wheel to rotate around a smooth profile, instead of threads. Threads would damage the plastic hub as the wheel rotates on taxi, takeoff, and landing.

The placement of the hollow interior of the assembly for the spring was made to maximize the contacting surface area between the upper and lower cylinders near the bottom of the assembly. Since the maximum stroke length was known, the mechanics of the mechanism were validated for minimum and maximum stroke in Catia, ensuring there was to interference between parts. For a maximum stroke of 1.5", the distance between the top of the outer cylinder and the fillet on the fuselage mounting plate of the inner cylinder was sized to a minimum of 1.65". An image of both MLGs assembled is shown in below. Each component and their masses are listed in Table 5 below.

Figure 15: Assembled MLG front (left) and back (right)

Table 5: Component list for a single assembled MLG with masses

Component	**Quantity**	**Purpose**	**Weight [g]**
Outer Cylinder	1		72
Inner Cylinder	1		53*
Spring	1	K=95[lb/in]	50
M4x12mm SHCS	4	Mounting inner cylinder to fuselage	10.13
M4 Flat Washers	4	Mounting inner cylinder to fuselage	
M4 Split Washers	4	Mounting inner cylinder to fuselage	
M2x8mm SHCS	1	Shear Bolt preventing rotation	
M3 Flat Washer	2	Reducing friction between wheel other components. One between wheel and M3 head, and one between wheel and outer cylinder	
M3 Hex Nuts	2	Two used together on the counterbore side of the outer cylinder. These can be tightened against each other to reduce loosening from vibrations.	
M2x8mm Heat Set Insert	1	Set into the inner cylinder for fastening the shear bolt	*weight included in inner cylinder
M3x65mm Partially Threaded SHCS	1	Axle and fastener for wheel assembly (bolt head on wheel side)	4.87

1” Hose Clamps	2	For clamping the outer cylinder to the inner cylinder, providing frictional damping. Placed above the wheel on the small diameter of the outer cylinder	39
R1.18” Foam Tire	1		9
Total MLG Assembly Mass (for one gear)			**238**

3.3 NLG Design

To save resources, namely time and money, it was decided to repurpose the purchased nose gear strut from the 2018-19 BWB UAV team. It is believed this strut was purchased from JP hobby, but the exact model is no longer available online [8]. Due to this, damping and shock characteristics for the strut are not known.

Due to the resizing of the MLG for the propellor clearance, the height of the NLG was required to be larger. To satisfy the height requirement, an extension was designed to bridge the gap between the purchased NLG and the mounting location on the fuselage. A preliminary version of this extension is shown below in Figure 16.

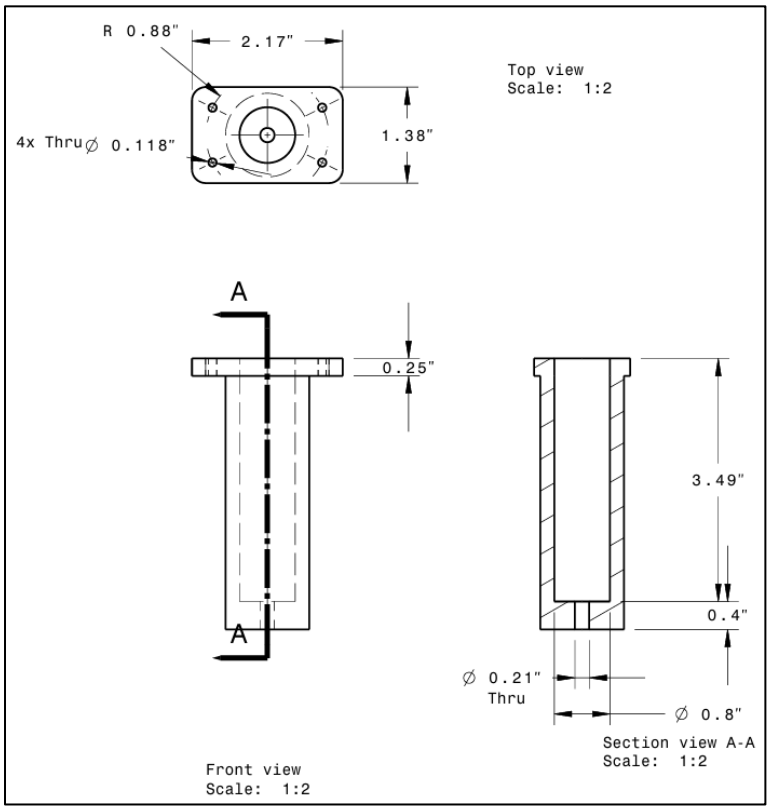

Figure 16: Engineering Drawing of NLG Extension

Figure 16 shows the hollow extension, with a hole for the pin that is attached to the purchased gear. The pin is pushed through from the inside of the extension and protrudes out the bottom, providing the

attachment point for the purchased gear. The fuselage mounting profile is the same as is used on the MLG, but rotated 90°, matching the approximate profile of the previous years mounting profile.

3.3.1 Torque Link

A torque link is a component of an aircraft landing gear that restricts relative rotational movement between the concentric piston cylinder and outer cylinder of an assembled strut [16]. This is demonstrated in Figure 17.

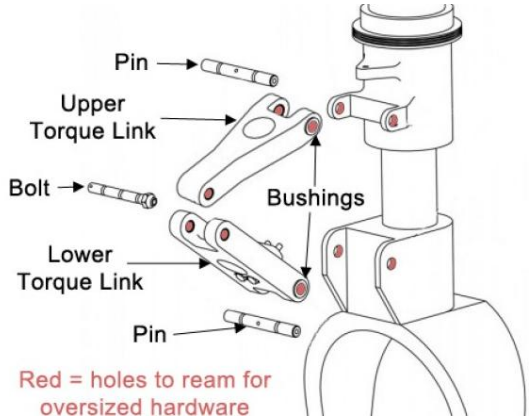

Figure 17: Torque link diagram for the Cessna 208 [17]

Since the pin that fastens the purchased NLG to the NLG extension is circular, the landing gear rotates freely around the axis of the pin. Due to this free motion, a torque link was required to keep the nose gear pointed forward. A torque link was constructed by fastening a 1” long piece of the metal strapping that came with the hose clamps to a heat set insert on the exterior of the NLG extension and a M2 bolt into the female threads present on the purchased NLG. A picture of the hose clamp strapping is shown below for reference.

Figure 18: Metal hose clamp strapping [18]

The slots in the metal strapping are used to fasten the SHCS to the extension and the purchased strut. The exact rotational position of the strut can be finely adjusted by moving either bolt to the left or the right of their strapping slot and then fastened tightly to sinch the strapping between itself and the part. The

clamping strength in this configuration was never validated. Shock loads could cause the strapping to slip from its exact position causing the aircraft to veer off course.

Soon after this assembly was made, the requirement of a steerable NLG was introduced, and the torque link was no longer applicable.

3.3.2 Structural Considerations

Similarly to the MLG, the type of loading experienced in a vertical gear should be mostly buckling. The landing attitude of the aircraft will affect how much of the initial loading acts in bending, as any attitude other than 0° to the horizontal will impart a small bending component into the gear. During the design phase, this parameter was not known, and the assumption was made that the attitude for the Peregrine 1, with its conventional takeoff and tricycle landing gear configuration, would be less than 5° and the concerns of bending would be negligible compared to the buckling load.

To mitigate concerns of the extension fracturing where the small diameter purchased gear contacts the extension, an oversized 3/8” inner diameter flat washer was incorporated to distribute this point force into the entire face of the NLG. Most importantly, this washer extends to the outer edge of the extension, so that the load may be transferred as compression through the extension walls, rather than in shear at the bottom most portion of the extension.

A large fillet was incorporated between the fuselage mounting bracket and the strut, and between the strut walls and the bottom horizontal section, to reduce stress concentrations in the additively manufactured part.

3.3.2 Final NLG

The final iteration of the NLG is shown below in Figure 19. 3mm Al6061 rod, initially purchased for the elevon linkage, was used as an axle. Two M3 clamping bolts were used to secure the axle in place. The masses of components are shown below in Table 6.

Table 6: NLG assembly list with component masses

Component	**Quantity**	**Purpose**	**Weight [g]**
Purchased NLG Strut	1		53
M3 clamping bolts	2	To secure the axle in place	
3mmx1.5” Al6061 axle	1	An axle for the	
2” diameter wheel	1		
3D printed extension	1	Increases the height of the purchased NLG strut	48
M4 Flat Washers	4	Mounting inner cylinder to fuselage	7
M4 Split Washers	4	Mounting inner cylinder to fuselage	
M2x8mm SHCS	1	Shear Bolt preventing rotation	
Total NLG Assembly Mass			**108**

Figure 19: NLG assembly diagram

3.4 Drop Test and Failure Modes

On the assembled NLG and MLG, a drop test was performed by the Loads Engineer. Information regarding this test should be sought from the Loads Engineer Winter Technical Report, but key findings are presented here.

From the first drop test, no additional loading was applied to the drop apparatus. The estimated load experienced by the aircraft was 12G, although a discrepancy between expected deflection of the MLG spring and the actual deflection of the spring was recorded. From video footage, the spring with a stiffness of 54 [lb/in] experienced little deflection, while under loads of 12G it should have bottomed out.

This first test also shows a flaw with the NLG assembly. Due to an unsecure connection between the extension and the purchased strut, there is deflection in bending of the NLG, shown below.

Figure 20: Drop test 1 pre-impact (left), mid-impact (middle), and max rebound post-impact (right)

The MLG can be seen with little to no deflection. The NLG can be seen forced forward due to the geometry the tire has relative to the strut.

The second drop test had an applied loading of 20kg on the drop fixture. The deflection of the MLG can measured from videos as 1.58”, indicating the spring completely bottomed out. During this loading, the MLG structure remained rigid other than at the fuselage mounting point. The NLG experienced an immediate and significant deflection forward, and the extension fracture due to the bending load. It is hypothesized that if the NLG had not failed causing the platform to pitch forward onto its nose, the MLG would not have failed at the mounting location. From the videos, the MLG supports all the weight and begins its rebound, at which point the NLG failed and the entire platform pitched forward while the MLG remained vertical. This can be seen below.

Figure 21: Drop test 2 MLG failure (from left to right: pre-impact, max deflection, fracture, max rebound)

The fracture pattern of the gears is shown below.

Figure 22: MLG Fracture

Figure 23: NLG Fracture

To mitigate these failure modes, the NLG design must be altered. Additionally, the fuselage mounting points of the MLG may be reinforced with a larger fillet or thickness.

3.5 Steering Mechanism

One week before the first flight test, members of the flight crew conducted a survey of the flight location. During this survey it was determined that the runway was too narrow, and in too poor of condition, to ensure that a fixed gear would maintain its heading before reaching the required speed for takeoff. It was feared that cracks in the runway would cause the platform to bounce off its course and head towards the grass ditch. A steering system was requested for implementation before the first flight test.

This mechanism was designed in 2 days and all components needed to be able to be sourced within 2 days to allow for assembly and testing. Recommendations are included for this assembly that were not able to be completed due to the extremely short development time.

3.5.1 Methodology and Linkage Design

It was decided that the easiest way to provide steering actuation for the NLG was to have a servo motor direct drive the free rotating purchased strut, with the torque link omitted. Small qualitative tests were performed on the rotational strength of the 3mm aluminum rod that was purchased for the elevon linkage. This proved to be far too weak, deforming easily. Once it was verified that there were rotary shafts available for purchase that were of a reasonable size for the assembly, CAD modelling began to prove out the assembly and parts needed to connect everything. An isometric view of the CAD model is shown in Figure 24.

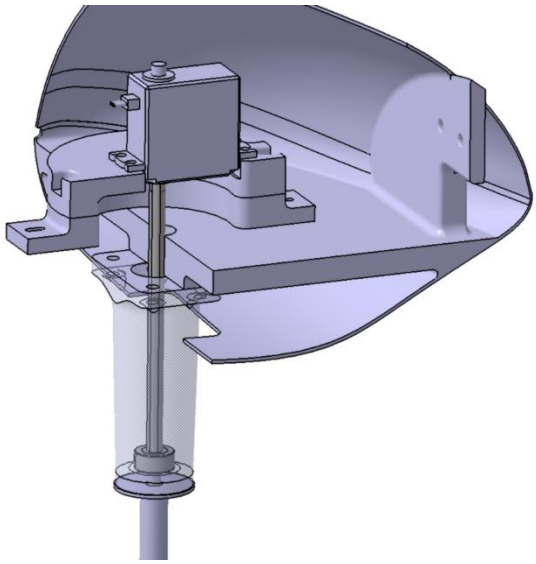

Figure 24: Steering mechanism isometric view

A 1/4” rotary shaft was determined to be the closest size to the purchased NLG pin, which is 0.275” in diameter. JB Weld was considered for the purpose of joining the shaft and the purchased NLG pin together but was decided against due to the permanent nature of the bond. If the connection was made incorrectly, or the purchased NLG was desired to be used in a different assembly later, the JB Weld would not be able to be removed. To satisfy the requirement of a zero-backlash connection between the shaft and the pin, a 1/4” D-profile collar was purchased. In the suite of rotary shafts available for next-day shipping from McMaster-Carr, D-profile shafts were available. The pin on the NLG would have to be machined down to

a quarter inch, and a D-profile would need to be added. With more time, this is a simple task. On a lathe, a finishing carbide insert can reduce the profile from 0.275” to 0.25” in a few seconds. In one pass, a milling machine could remove the material to make the pin have a matching D-profile to the collar. Unfortunately, due to the time constraints and a busy machine shop, this was done manually with an angle grinder fitted with a grinding wheel, the result of which is shown in Figure 25.

Figure 25: Alterations made to the purchased NLG pin

0.001” aluminum shim tape and 0.002” aluminum shim stock was purchased alongside the other components in the event of an error during the modification of the NLG pin. Shims are thin strips are material used to align parts or alter the fit of assemblies. If too much material was taken off of the OD of the pin, a shim could be placed between the pin and collar to fine tune the fit.

From the servo side, there were two considered options. The first option was to use the M3 threads that went directly into the servo. For the assembly to not unscrew itself, the male M3 threads would need to be permanently fixed into the servo, effectively rendering the servo useless for anything else. The second option was to purchase a metal servo horn and assemble it to another component that would sit perfectly concentric to the rotation of the servo. From McMaster-Carr, the options for a suitable component that would be used to connect to the servo horn described in option 2 included a circular profile and square profile adhesive ready nuts. These are shown in Figure 26 below.

Figure 26: Adhesive-ready nuts, M4 square (left) and circular (right) profile

From the engineering drawings of the circular profile nuts from McMaster-Carr, the ability to assemble them to a round 25T servo horn found on Amazon Canada was evaluated. These servo horns are shown in Figure 27 below.

Figure 27: Aluminum 25T round servo horns

The fit between the round servo horns and the round square profile nuts was very close to not able to be assembled as desired, so the square profile adhesive ready nuts were purchased as a backup plan. The plastic servo horns that were in the BWB UAV teams' inventory could have holes drilled out to the size of the outermost holes of the square-profile nuts. This was less desirable than using the metal servo horn due to the ability for the plastic servo horns to strip at their connection to the servo or plastically deform under the shock loading in the gear.

Once the assembly method between the rotary shaft and NLG was decided, and the hardware connecting the servo to the nuts was determined, the connection between the shaft and the adhesive-ready nuts was considered. From McMaster-Carr, the most promising rotary shaft that would allow further components to be easily connected that also fit the requirements of D-profile and 1/4" diameter was one that was tapped at one end. Unfortunately, the thread size in this shaft was 5-40, which is a very uncommon thread size and pitch. To connect a female 5-40 thread to a female M4 thread should be one thread adapter, but due to the obscurity of 5-40 threads, this was not readily available. A solution was found by the Master Additive Engineer, Tim Speyer, by using gun cleaning fitting adapters. Luckily, 5-40 is a standard thread for shotgun cleaning rods. A pack of adapters were purchased, displayed in Figure 28 below.

Figure 28: Various thread adapters

From the available adapters, it was determined that if a permanent connection had to be made directly into the servo, the assembly would consist of the female 5-40 threads on the shaft, a male 5-40 to female M3 adapter, a male M3 to male M3 adapter, which would directly fit screw into the servo. If the aluminum servo horn and adhesive nuts were successful, the assembly would follow female 5-40 threads on the shaft, male 5-40 to female M4 adapter, male M4 to male M4 adapter, which would screw into the M4 adhesive-ready nut. Since there was only one of each adapter within the set, it is beneficial that these assemblies are not mutually exclusive since each connection needed to be permanently joined.

The method of permanent joining was with Loctite 638, which is a retaining compound designed for bonding cylindrical fitting parts filling gaps between 0.15 and 0.25mm. The shear strength of the compound once cured is 4500 psi [19]. Loctite 222, a low strength thread locker, was also suggested by the author to the Assembly Engineers for use on all structural bolt connections to prevent loosening from vibrations. These two products are shown below in Figure 29.

Figure 29: Loctite 222 and Loctite 638

The last alteration that was considered for the assembly to be successful was the length of the rotary shaft. The smallest length available was 6”. From the CAD model, the length required length was between 2-4 inches, depending on the positioning of the servo.

Figure 30: Marks being made to size the rotary shaft prior to being cut

With more time, this would have been done in a lathe, with a parting insert. As before, the short notice made it essential for this manipulation of the part to be successful without a machine shop. Once it was

confirmed that a cut-off disk for an angle grinder could be sourced, all the components for the steering mechanism were ordered.

3.5.2 Produced Linkage

The produced linkage was the most preferred of all the solutions and backup plans. The aluminum servo horn was assembled to the round adhesive ready M4 nut. The male-male M4 adapter was used alongside the female M4 to male 5-40 adapter, which was threaded into the 5-40 tapped rotary shaft.

The pin was successfully brought from an outer diameter of 0.275 inches to approximately 0.25 inches. A piece of shim tape was required between the purchased NLG pin and the collar due to the D-profile grinded into the pin being slightly different than the profile of the collar. Each of these components were permanently joined with Loctite 638 and cured for 24 hours. The linkage is shown in Figure 31 below.

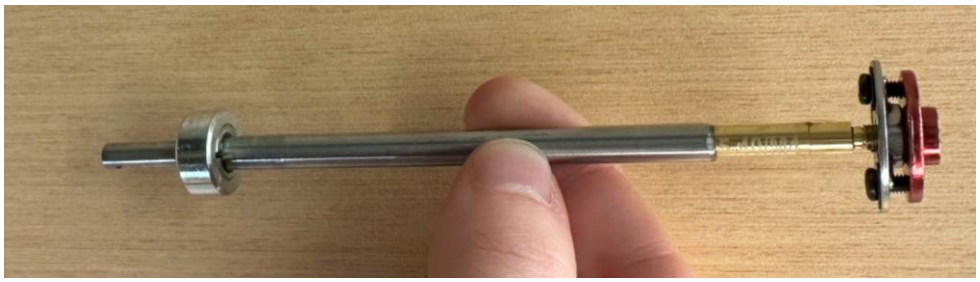

Figure 31: Steering linkage for additively manufactured platform

In addition to the linkage produced for the 3D printed platform, an additional linkage was constructed for the foam model. A day before the flight test, it was decided that it would be too risky to proceed with flying the 3D printed model due to unfinished 3D printed pieces and an incomplete assembly. Due to the different landing gear geometries, the D-profile rotary shaft was not required for this linkage. Instead, several adapters were chained together and the largest adapter at the end of the chain was grinded down to a D-profile, to fit into the collar. This assembly was prone to slippage due to the improper connection between the adapter and collar but was temporarily fixed with shim stock during the first flight test. The foam model steering shaft is shown assembled into the foam model landing gear assembly in Figure 32 below.

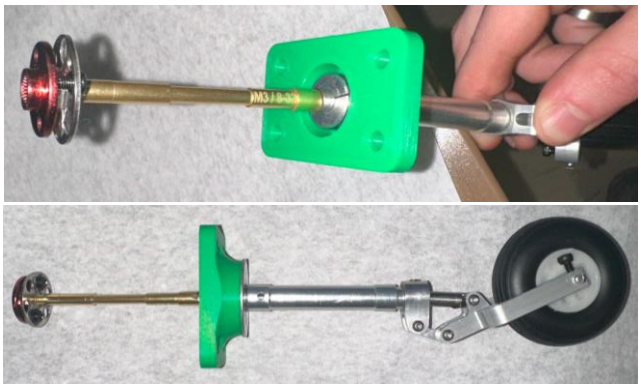

Figure 32: Foam model steering linkage assembled

3.5.3 Servo Mount

The final part to be designed for the successful integration of a steering system was a mount for the servo motor. By reverse engineering a drawing for the servo motor, a mounting bracket was designed around the model, to secure the servo in place and allow it to resist deflection from torsion of the gear.

The mount was designed in three pieces. The upper mount is what the servo was mounted to, with 4 M3x6mm heat sets inserts allowing four M4 SHCS to clamp the servo bracket. The upper mount was fastened into a lower mount through the use of two M4 bolts which were fastened from the upper mount into M4 heat set inserts installed in the lower mount. Figure 33 shows the upper mount with the servo installed.

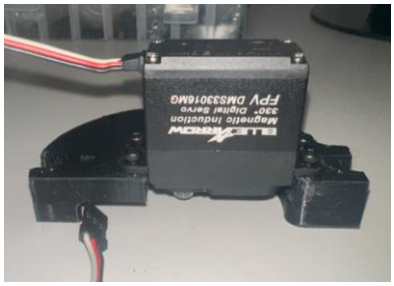

Figure 33: Steering servo installed on the upper mount

The lower mount is fastened to the fuselage through two M3 bolts that thread into two M3 heat set inserts installed into the floor of the fuselage. The third component are a series of spacers that can be added or removed to change the height of the servo. The reasoning for this design choice was that when the rotary shaft is cut to size, there is a risk factor of the sizing not lining up perfectly. Since the mechanism is a direct drive setup, the vertical positioning of all components is critical. A gap of 0.1 inch introduced in any portion of the assembly would result in the servo horn not being able to be attached to the servo. Since the cutting of the shaft is a permanent alteration on a high-cost part, 0.05” spacers would servo as the fine tuning of the length of the assembly. If the shaft were cut slightly too short, a spacer could be removed, allowing the servo to maintain its contact with the shaft, or vice-versa. The steering assembly installed in the 3D printed fuselage is shown below. This also guided the selection of M4 SHCS being used to fasten the upper and lower mount together. The maximum length of the M4 screws that were readily available were 20mm compared to the 16mm M3 SHCS. The extra length would provide a larger safety factor of error for the sizing of the assembly, allowing more spacers between the upper and lower mounts.

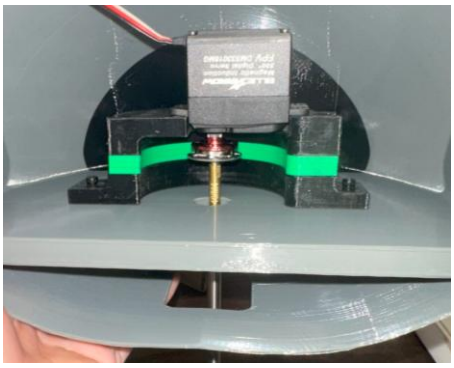

Figure 34: Steering mount assembly installed on 3D printed Peregrine 1

A modified design was implemented on the foam model due to foam not being a suitable material for heat set inserts to be assembled to. This design used #8x1.75” wood screws, fastened through the upper mount and spacers, that were screwed into the foam where the M4 bolts were originally designed to be placed. A liberal application of duct tape was also employed to mitigate torsion in the assembly, shown below in Figure 35.

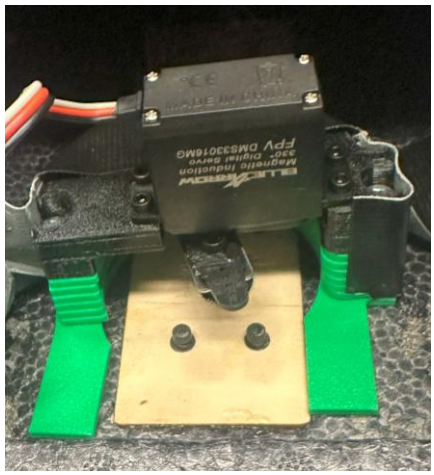

Figure 35: Steering servo mount installed on foam platform

Figure 36: NLG installed on foam platform

The final assembly of the NLG with the steering system, installed on the 3D printed platform, was very successful in ground tests.

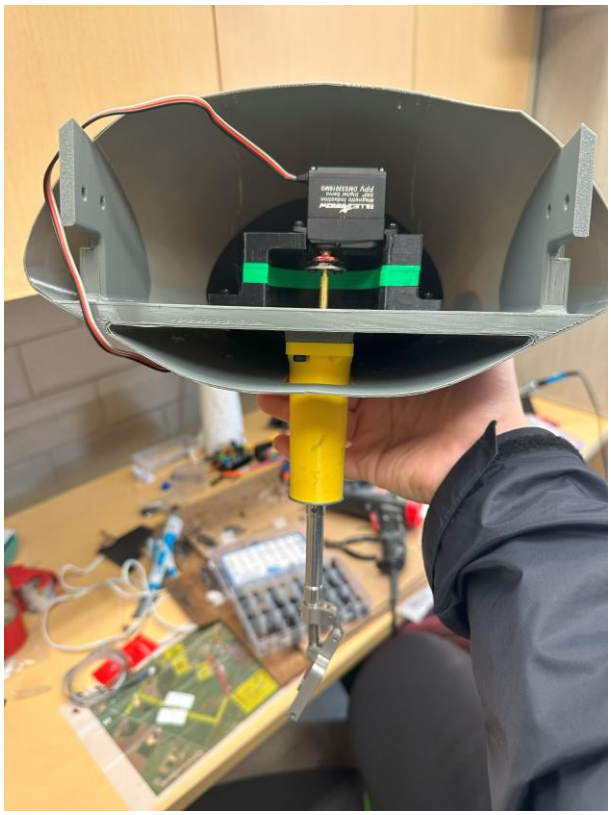

Figure 37: NLG and steering system installed on the 3D printed Peregrine 1

3.5 Next Steps and Recommendations

The implementation of the custom MLG was very successful. Efforts could be made to reduce the mass of the gear by performing a proper stress analysis on the structure, using energy methods and FEA. Additionally, the mathematical characterization of the behaviour of the shock absorber, including determination of the damping characteristics imparted from the friction between the inner and outer cylinder, would be beneficial.

For the future, it is recommended that resources are spent redesigning the NLG, due to its critical design flaw of a weak connection between the extension and the purchased NLG. The purchased NLG should no longer be used due to its wear. The oleo struts have leaked all their fluid from repeated testing and use. The shock characteristics are now much weaker than the rated design.

All three wheels used in the landing gear assembly should be reevaluated. The wheels selected for the current year were carried over from the 2018-19 year, when the last conventional model was pursued. Their deflection under the static weight of the aircraft is concerning.

For the steering system, a gearing mechanism should be used between the servo and the steering linkage. This would serve two main purposes. The first is to prevent the NLG being able to backdrive the servo motor. When the gear hits an unsymmetrical bump in the runway, a large torque force is impacted into the mechanism. In the current design, it is entirely possible that this force is enough to force the servo to

move, causing misalignment issues and discrepancies between the flight controller positioning of the steering servo and the actual positioning of the steering servo. A mechanism like a lead screw is very good at preventing backdriving. The second purpose is to aid in the fine positioning of the servo. The 330° servo used uses only 6% of its available motion range to move the servo -10° to +10° from the centerline. This is very inaccurate which was seen in taxi tests, where constant adjustment of the steering was required to keep the aircraft straight. A gearing ratio can allow more of the available range of the servo motor be used for the required range of motion for the steering.

4.0 CONTROL SURFACES

Integration of the control surfaces to the airframe and avionics is critical to the success of the mission. On the BWB UAV, there exists only a left and right elevon – a combination of the elevators and ailerons. The assembly methods and design of the elevon to incorporate the new design are described in this section. Additionally, a new elevon linkage was designed to better align with the mission goal of manufacturing the Peregrine 1 with additive manufacturing.

4.1 Elevon to Airframe

Prior to the current objective of an additively manufactured aircraft, the installation of the Peregrine 1 control surfaces was done with an aluminum rod that passed directly through the axis of rotation of the elevon, connecting to the wing on each side of the elevon. To reduce the weight of this assembly, plastic hinges were recommended by drone enthusiasts in the capstone group.

Within a CAD assembly, shown in Figure 38 and Figure 39, the mechanics of the new hinge integration were evaluated. It is desired to keep the axis of rotation of the elevon from the aluminum rod design, the same as with the hinges. This serves to preserve the mechanics and aerodynamics of the control surfaces, which is established as a fixed design constraint.

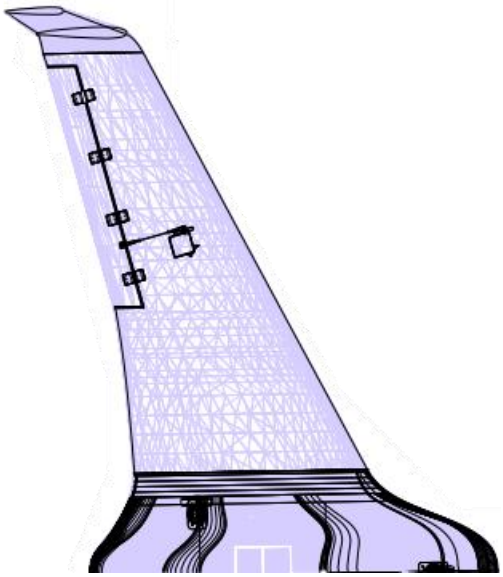

Figure 38: Top view of the elevon assembly integrated in the wing

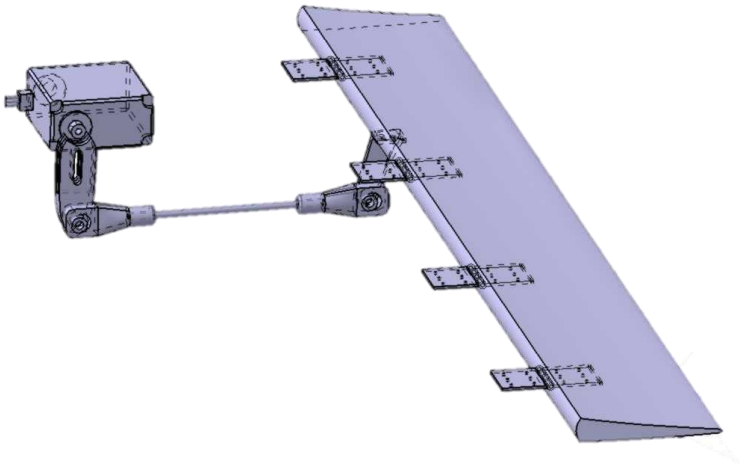

Figure 39: Isometric view of elevon hinge and linkage model

4.1.1 Hinge Validation

Tensile testing was performed on the elevon hinges to validate their strength. For the test, the hinges were sinched between two metal plates on both sides, shown in Figure 40.

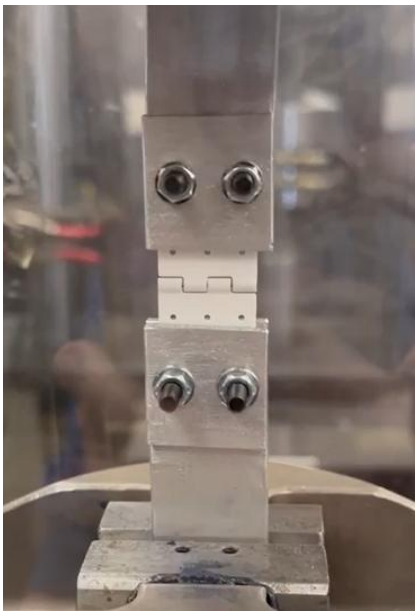

Figure 40: Hinge tensile test fixture

A speed of testing of 6 [mm/m], 60 [mm/m] and 20[mm/m] were each used on a single specimen. From this initial testing, it was observed that at 60[mm/min], brittle fracture occurred within 3 seconds, with a reduced ultimate loading versus the other rates of testing. At 6[mm/s] the load peaked at 10 seconds, but fracture never occurred. A third strain rate of 20[mm/s] was tested, which yielded a similar ultimate load, but fractured within 12 seconds. From this initial data, a rate of testing of 20[mm/m] was selected.

Three samples were tested, yielding an average ultimate load of 217 [N].

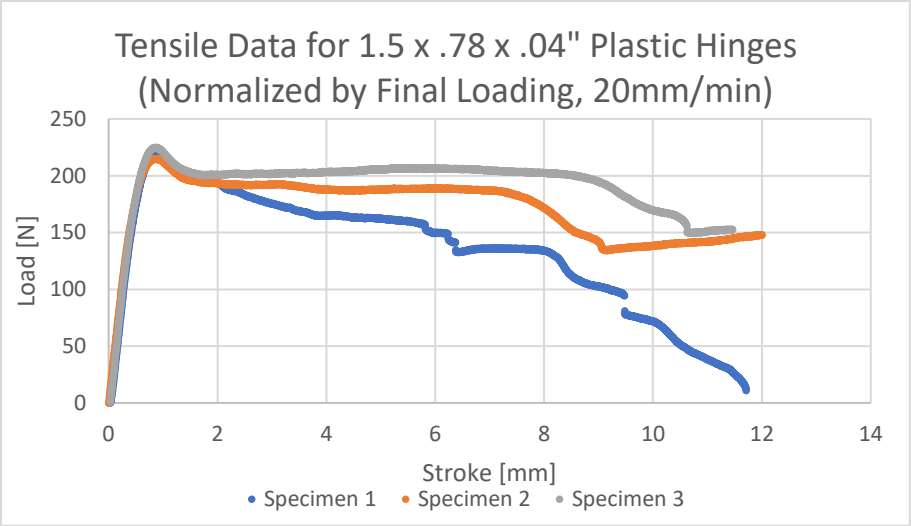

Figure 41: Load versus Stroke for hinge tensile testing

A stress versus strain graph could not be constructed from the data due to inconsistent failure mechanisms and variable failing cross sectional areas, shown in Figure 42.

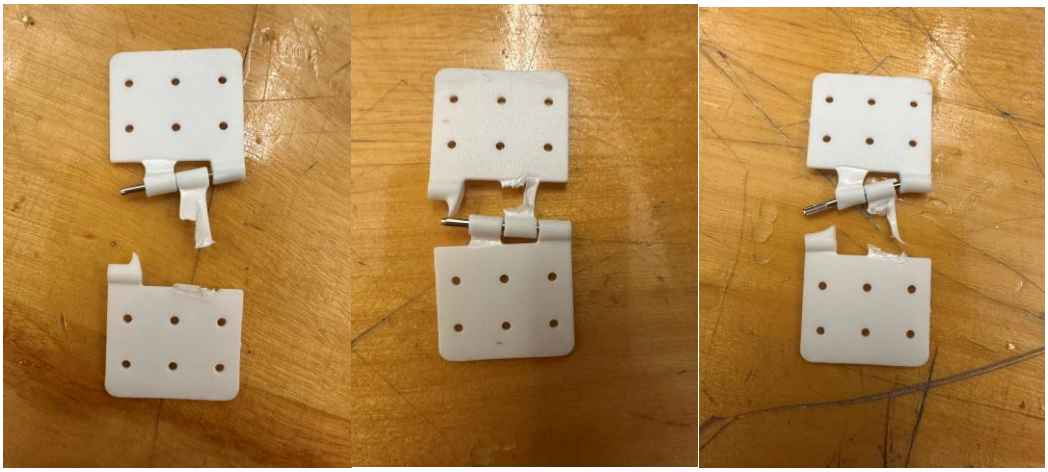

Figure 42: Failure in specimen 1 (left), specimen 2 (middle) and specimen 3 (right)

An analysis of estimated loads experienced on the elevon is presented in section 4.2.1. From this analysis, only a portion of the estimated 16.6 [N] acting on the elevon will be experienced in all four hinges combined. The hinges are determined to be safe for the current mission profile.

4.2 Elevon Linkage

It was decided that having multiple sets of linkages would be beneficial in the event of a linkage failure or accidental breakage. To align with the mission goals of an additively manufactured aircraft and to save money on duplicate sets of store-bought linkages, a custom solution was pursued. The elevon linkage was modelled after the previous store-bought linkage, using 3mm diameter aluminum bar as the connecting rod. To facilitate the free rotation of the aluminum bar connectors with the servo and elevon horns, an

M2 heat set insert was installed in axis of rotation of the connecting rod and the horns. An M2 SHCS with an M3 and M4 washer held the linkage rod connectors in place. The heat set insert assembled components are shown in Figure 43.

Figure 43: Custom elevon linkage subassembly front (Left) and side (right) views

Many iterations of this design were completed to arrive at the final version shown above. Within the largest component in Figure 43, the servo horn extension, a 25T servo horn is attached with two M2 SHCS. This alteration was made to eliminate plat between the servo horn extension and the servo. The additional length from the servo horn extension allowed the four-bar linkage to keep its desired proportions, ensuring that for a given servo deflection, the resulting elevon deflection was equal.

The motion of the linkage was verified with a graphical kinematic analysis, shown below.

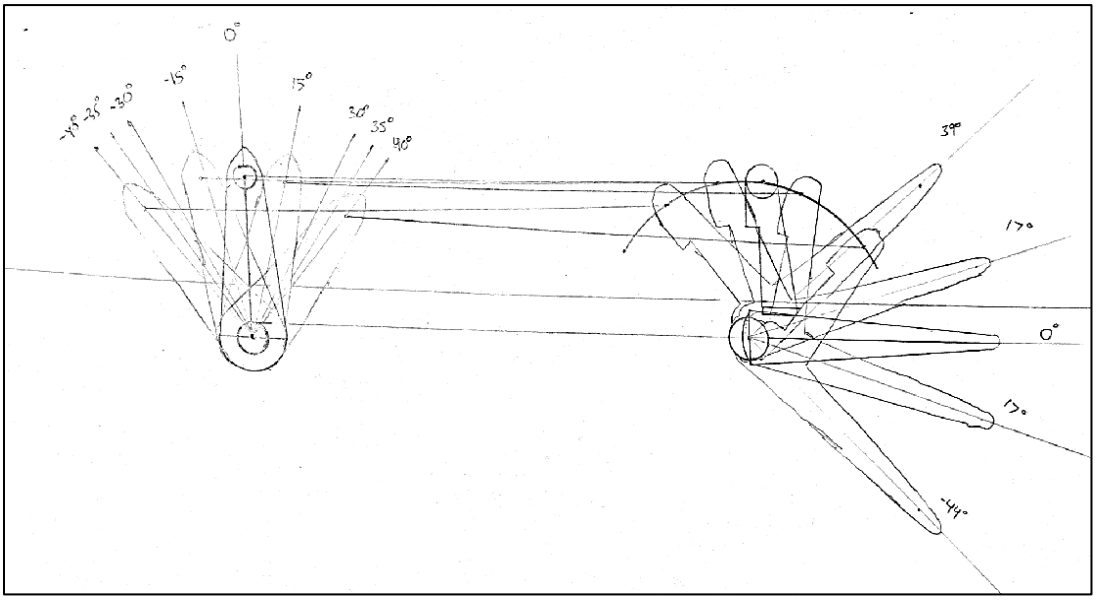

Figure 44: Kinematic analysis performed on linkage movement

This analysis identified a problem that the elevon horn was introducing into the linkage. Due to the set back pivot point of the elevon horn to rod connection relative to the rotational axis of the elevon, compared to the vertically inline position of the servo rotational axis and the servo horn and rod pivot point, the resulting motion showed a non-linear input response. From Figure 44, for a +40° servo

deflection, the elevon deflection was -44°. For a -40° servo deflection, the resulting elevon deflection is 39°. This issue was rectified in the next iteration of the linkage, by translating the elevon horn rotational axis to the left in Figure 44. This change can be seen in Figure 43.

4.2.1 Linkage Rod Stress

To verify the strength of the linkage, an estimate of the load present in the assembly was estimated. Using the drag force equation, shown below, the force that the air imparts on the elevon can be estimated.

$$F = \frac{1}{2} C_D \rho V^2 A \qquad 4$$

In Equation 4, C_D is the coefficient of drag, ρ is the density of the air, V is the velocity of the air, and A is the frontal area of the object in the flow as seen from the direction of the freestream velocity. For this approximation, a few assumptions were made. Firstly, the maximum load on the linkage would be seen if the elevon was at its maximum deflection. The support from the hinges was neglected for the initial load calculation. C_D was estimated to be 1.3, where $C_D = 2$ is used for a bluff body, and aerodynamic bodies have a coefficient of drag between 0.3 and 0.5. Lastly, the elevon was assumed to be rigid.

From the platform geometry, the frontal area of the elevon at a 45° deflection was calculated as 0.01774m^2. The density of air at standard conditions is 1.225 [kg/m^3]. The freestream velocity was received by the performance engineer as 34.3 [m/s]. From these parameters, the load acting at the geometric center of the elevon was calculated as 16.6 [N].

The two-dimensional static mechanics problem in Figure 45 was constructed containing the elevon at 45 degrees, the load from the freestream velocity acting parallel to the freestream at the geometric center of the elevon, the elevon horn perpendicular to the elevon at 0.5 inches from the pivot point of the elevon, and the linkage rod parallel to the freestream.

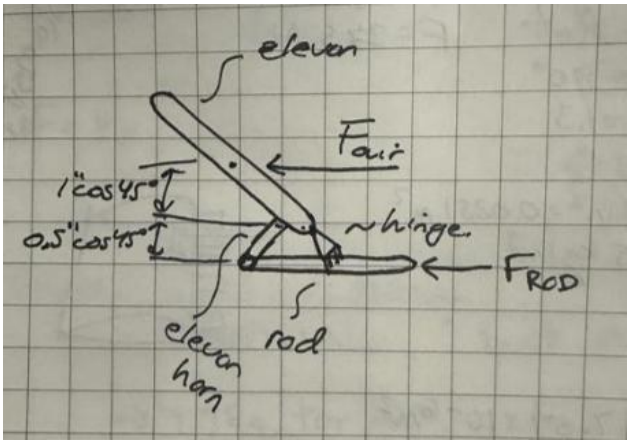

Figure 45: Static analysis of elevon linkage loads

A sum of the moments acting about the elevon hinge yields a force in the rod of 33.54 [N]. With $\sigma = \frac{F}{A}$, the stress in the rod was calculated as 4.74 [MPa]. The aluminum alloy used in the rod is Al6061, which has a yield stress of 110 [MPa]. This represents a safety factor of 23 for the rod to the air loads which is satisfactory.

4.3 Wind Tunnel Testing

The author pursued the use of the wind tunnel for elevon deflection verification. It was proposed to the Aerodynamics Engineer that a mount could be constructed to hold the aircraft in place, aerodynamic data could be retrieved, and a validation of the elevon servo and linkage strength could be conducted.

Due to time limitations, the avionics were not installed for the wind tunnel test. Instead, the elevon linkages were fixed in 35°, 0°, and -35° positions for three different wind tunnel tests. From qualitative observations, no deflection or deformation of the linkage was observed for a freestream velocity of approximately 24 [m/s].

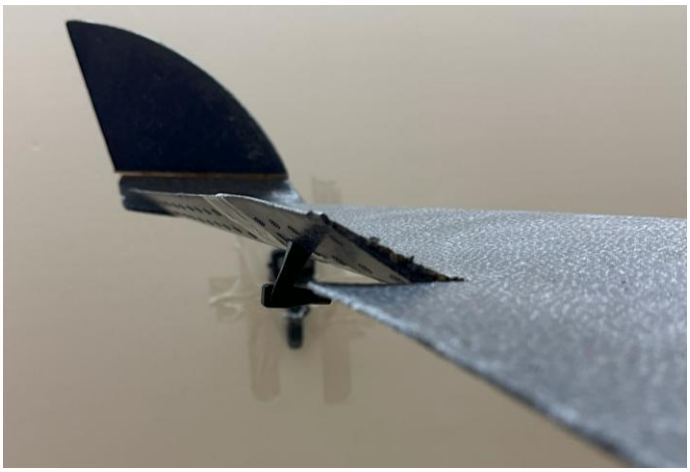

Figure 46: Elevons linkage fixed in 35° deflection for wind tunnel testing

Figure 47: Elevons fixed in -35° deflection for wind tunnel testing

For more information on the wind tunnel testing procedure, and the mounting apparatus shown in Figure 48, see the Aeordynamics Engineer Winter Technical Report.

Figure 48: Overall wind tunnel testing setup

5.0 CAD MODELLING

Due to the work that was done by the author on the masterlines CAD model in the fall, a good understanding of the platform model was gained. Due to this, assistance was provided in modelling throughout the course of the semester, when requested.

5.1 Elevon

To integrate the slots required for the hinges into the elevon, the elevon model was constructed by the author. A picture of the supplied model was shown in Figure 39. It was also advised by the author that slots were to be made above and below each elevon slot, as shown in Figure 49, but this design was never implemented.

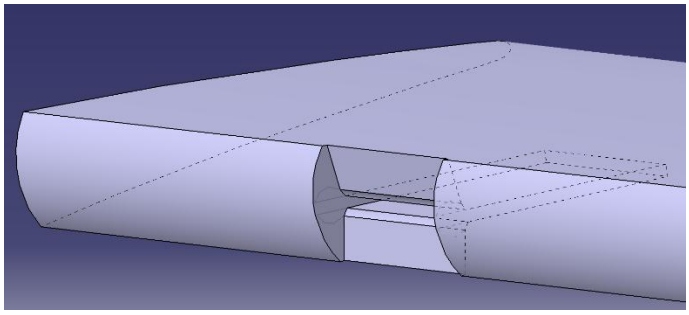

Figure 49: Elevon slots above and below each hinge to address clearance issues

The purpose of these slots was to address clearance issues between the hinge and the elevon. For the axis of rotation of the hinge to be preserved from previous years designs, the rotation axis of the hinge needs to be inset into the elevon slightly.

5.2 CFD-Oriented CAD Model

The Aerodynamics Engineer requested changes to be made to an early iteration of the model, to allow for successful modelling using CFD. An image of the model provided is shown below.

Figure 50: CAD-Oriented CAD Model provided to the Aerodynamics Engineer

This model contains early revisions of the landing gears and the assembled elevon linkage. The model also has the elevon deflection constrained, allowing the deflection angle to be changed with a parameter, as requested by the Aerodynamics Engineer.

The model was made through several revisions with the Aerodynamics Engineer. For CFD models, it was understood that all components needed to be in contact for the software to register it as a single body.

5.3 BWB UAV Catia Modelling Practices

A document was produced titled *BWB UAV Catia Practices* which describes, in more detail than *TM-P1CatiaModellingPractices-EithinPero,* recommendations for future development on the Catia model. It is recommended that this document is read by future Masterlines Engineers.

6.0 CONCLUSION AND RECOMENDATIONS

The progress of the required deliverables was very successful in the winter semester. A few scope changes, primarily regarding the paused development of a retractable landing gear and the shift away from viscoelastic materials as a spring and shock mechanism were made due to high workload pursued by the Systems Engineer 2.

6.1 Mapping Module

The integration of the mapping system through the development of the mapping mount was successful. Future years should conduct a vibration analysis on the impact of the camera footage. Although the mount

was designed to isolate the camera from aircraft vibrations, this should be validated through empirical and vibration testing.

Additionally, hard wiring the camera into the Peregrine 1 power supply will allow for longer endurance mapping to be conducted. Finally, a PWM trigger should be purchased to facilitate the capture of images from the flight controller.

6.2 Landing Gear System

In the pursuit of a landing gear system, many items were delivered. A custom MLG fitted with a compression spring and frictional damping was created. From loads testing, the design of this gear is adequate for the current mission profile. Efforts could be made to further understand the behaviour of the shock and loads seen within the gear, making small revisions accordingly.

For the NLG, two configurations were produced. A full-scale extension and an attachment method between the extension and the purchased gear was provided. Additionally, a small-scale extension with a similar attachment method was produced for the foam model. A design flaw persists where the connection between the purchased NLG and the additively manufactured extension is unsecure. This introduces high bending loads into the gear on impact which caused the failure in shear during the drop test. Additionally, the pin on the purchased gear is now permanently fixed to the steering linkage and the strut has lost most of its shock resistance due to repeated use. This should be abandoned in favour of another custom solution.

The wheels on both the MLG and NLG should be resized as significant deflection was seen during the drop test. Lastly, the method of landing gear sizing should be reconsidered from scratch, using the now-known center of gravity for the aircraft. The egregious approximations used for the initial sizing in the current year are no longer required. Changes to the design should be made as required.

For the steering system, a successful iteration was produced for the additively manufactured platform. A successful, but delicate iteration was produced for the foam model. Issues with this design should be rectified with suggestions contained within section 3.5.

6.3 Elevon Integration and Actuation

In the realm of elevon integration and actuation, a successful integration of the elevon assembly method was produced by the Assembly Engineers, as per advice from the author. Elevon linkages were designed, manufactured, and validated. Additionally, the elevon servo connection into the wing was modelled successfully by the author. It was determined that the assembly has a high-risk step, where the elevon must be permanently joined to the hinges, while keeping all 4 hinges perfectly inline. This should be redesigned.

7.0 REFERENCES IEEE

[1] A. Bowers, "Blended Wing Body: Design Challenges for the 21st century," NASA, 200.

[2] MAPIR, "Survey3W Camera - Red+Green+NIR (RGN, NDVI)," MAPIR, 05 01 2025. [Online]. Available: https://www.mapir.camera/collections/survey3/products/survey3w-camera-red-green-nir-rgn-ndvi. [Accessed 31 3 2025].

[3] Share Goo, "ShareGoo Glass Fibre Shock Absorber Board," Amazon, 2025. [Online]. Available: https://www.amazon.ca/ShareGoo-Absorber-Anti-Vibration-Damping-Controller/dp/B072KB31YT/ref=asc_df_B072KB31YT/?tag=googleshopc0c-20&linkCode=df0&hvadid=706827341039&hvpos=&hvnetw=g&hvrand=1391238593897600531&hvpone=&hvptwo=&hvqmt=&hvdev=c&hvdvcmdl=&hvloci. [Accessed 31 3 2025].

[4] NASA, "NASA Engineering and Safety Center Technical Bulletin No. 15-03: Best Practices for Use of Sine Vibration Testing," National Aeronautics and Space Administration, 2015. [Online]. Available: https://www.nasa.gov/wp-content/uploads/2015/04/nesc-tb-15-03-best-practices-for-use-of-sine-vibration-testing.pdf. [Accessed 05 04 2025].

[5] AVIATION, "How does angle of incidence affect an aircraft's stability?," Stack Exchange, 2019. [Online]. Available: https://aviation.stackexchange.com/questions/51081/how-does-angle-of-incidence-affect-an-aircrafts-stability. [Accessed 03 04 2025].

[6] D. Raymer, Aircraft Design - A Conceptual Approach (seventh ed.), Reston, VA: Amer Inst of Aeronautics, 2024.

[7] Department of Transportation and Federal Aviation Administration, "Title 14, Chapter 1, Subchapter C, Part 23 - Airworthiness Standards: Normal Category Airplanes (23.925a)," 2025. [Online]. Available: https://www.ecfr.gov/current/title-14/chapter-I/subchapter-C/part-23. [Accessed 02 04 2025].

[8] JP Hobby, "Landing Gears Propellor Models," JP Hobby, 2025. [Online]. Available: https://www.jphobby.eu/en/275-landing-gears-propeller-models#/serial-jp_hobby_er_200_30kg. [Accessed 01 04 2025].

[9] E. Pero, "TR1-Systems2-EithinPero," BWB UAV Capstone, Carleton University, Ottawa, 2024.

[10] Q. Wei, "Systems Engineer - 2 Winter 2022 Technical Report," Dept. of mechanical and aerospace engineering, Carleton, Ottawa, 2022.

[11] P. T. R. Kumar and D. G. Ramakrishna, "Mechanical characterization of PETG-3D printed material for enhancement and scrutiny," *YMER Digital,* vol. 24, no. 2, p. 20, 2025.

[12] Transport Canada, "Flying your drone safely and legally," Government of Canada, 2025. [Online]. Available: https://tc.canada.ca/en/aviation/drone-safety/learn-rules-you-fly-your-drone/flying-your-drone-safely-legally. [Accessed 16 01 2025].

[13] Britannica, "damping," Britannica, 2025. [Online]. Available: https://www.britannica.com/science/damping. [Accessed 06 04 2025].

[14] The Complete Automobilist, "Andre Hartford Shock Absorbers," 2025. [Online]. Available: https://www.completeautomobilist.com/categories/ca-andre-hartford-shock-absorbers. [Accessed 02 04 2025].

[15] N/A, "Novel suspension for light aircraft," *Aircraft engineering and aerospace technology,* vol. 72, no. 1, pp. 67-68, 2000-01.

[16] A. Krisbudiman, "Structural Design Analysis Torque Links of Nose Landing Gear on light aircraft," *International jounral on Advanced Science Engineering Information Technology,* vol. 14, no. 2, pp. 507-514, 2024.

[17] Airforms.biz, "C208/C208B Torque Link Repair STC," AIRFORMS, 2025. [Online]. [Accessed 04 2025].

[18] Homagic, "Hose Clamp Stainless Steel DIY 7.9 FT Metal Strapping with Holes," Amazon, 2025. [Online]. Available: https://www.amazon.ca/Fasteners-Stainless-Adjustable-Clamps-various/dp/B092CN53R7?th=1. [Accessed 06 04 2025].

[19] Loctite, "LOCTITE 638," Henkel, 2025. [Online]. Available: https://www.henkel-adhesives.com/ca/en/product/retaining-compounds/loctite_6380.html. [Accessed 07 04 2025].

[20] McMaster-Carr, "McMaster-Carr Catalog," 2024. [Online]. Available: www.mcmaster.com. [Accessed 20 10 2024].

[21] Q. Wei, "SYSTEMS ENGINEER - 2 FALL 2021 TECHNICAL REPORT," Dept. of Mechanical and Aerospace Engineering, Ottawa, 2021.